12270–12284 *Nucleic Acids Research, 2017, Vol. 45, No. 21* *Published online 3 October 2017*
doi: 10.1093/nar/gkx831

hnRNPM guides an alternative splicing program in response to inhibition of the PI3K/AKT/mTOR pathway in Ewing sarcoma cells

Ilaria Passacantilli[1,†], Paola Frisone[1,†], Elisa De Paola[1,2], Marco Fidaleo[1] and Maria Paola Paronetto[1,2,*]

[1]Laboratory of Cellular and Molecular Neurobiology, Fondazione Santa Lucia, Via del Fosso di Fiorano, 64, 00143 Rome, Italy and [2]University of Rome 'Foro Italico', Piazza Lauro de Bosis 6, 00135 Rome, Italy

Received May 30, 2017; Revised August 18, 2017; Editorial Decision September 06, 2017; Accepted September 12, 2017

ABSTRACT

Ewing sarcomas (ES) are biologically aggressive tumors of bone and soft tissues for which no cure is currently available. Most ES patients do not respond to chemotherapeutic treatments or acquire resistance. Since the PI3K/AKT/mTOR axis is often deregulated in ES, its inhibition offers therapeutic perspective for these aggressive tumors. Herein, by using splicing sensitive arrays, we have uncovered an extensive splicing program activated upon inhibition of the PI3K/AKT/mTOR signaling pathway by BEZ235. Bioinformatics analyses identified hnRNPM as a key factor in this response. HnRNPM motifs were significantly enriched in introns flanking the regulated exons and proximity of binding represented a key determinant for hnRNPM-dependent splicing regulation. Knockdown of hnRNPM expression abolished a subset of BEZ235-induced splicing changes that contained hnRNPM binding sites, enhanced BEZ235 cytotoxicity and limited the clonogenicity of ES cells. Importantly, hnRNPM up-regulation correlates with poor outcome in sarcoma patients. These findings uncover an hnRNPM-dependent alternative splicing program set in motion by inhibition of the mTOR/AKT/PI3K pathway in ES cells that limits therapeutic efficacy of pharmacologic inhibitors, suggesting that combined inhibition of the PI3K/AKT/mTOR pathway and hnRNPM activity may represent a novel approach for ES treatment.

INTRODUCTION

Ewing sarcomas (ES) are aggressive tumors of bone and soft tissues mostly afflicting children and young adults (1). They are caused by chromosomal translocations that yield in-frame fusion proteins comprising the amino terminus of the Ewing sarcoma protein (EWS) fused to the carboxyl terminus of various ETS transcription factors. In 85% of the cases, EWS is fused to the Friend leukemia virus integration site 1 (FLI-1), less commonly to the ETS-related gene ERG, the ETS-variant gene 1 (ETV-1), the ETS variant gene 4 (ETV-4), and the fifth Ewing sarcoma variant (FEV) (2). EWS is a RNA and DNA binding protein that plays direct roles in splicing regulation and in the response to genotoxic stress (3–6), while FLI-1 is a member of the ETS family of transcription factors that binds GGAA-microsatellite elements embedded within promoter/enhancer regions of target genes (7). However, the EWS-FLI-1 fusion proteins resulting from chromosomal translocations are deregulated and trigger a specific oncogenic program that directs neoplastic transformation of ES cells (8).

A combination of surgery and radiotherapy, followed by chemotherapy, is still the only treatment for ES patients (9–12). Unfortunately, these treatments damage both normal cells and cancer cells, and in the long term have deleterious effects on tissues, resulting in learning difficulties, impaired hearing, vision and growth, as well as cardiovascular and respiratory problems in children affected by the disease. Moreover, most ES tumors relapse with distant metastatic disease following surgical resection (13), contributing to the poor prognosis of ES patients (11). Thus, alternative treatments and new markers for early diagnosis are urgently needed.

The PI3K/AKT/mTOR signaling pathway is often aberrantly activated in ES (14,15). This pathway plays a central role in the regulation of cell growth in various human cancers (16–19). Mitogens activate PI3K and AKT, leading to activation of a complex formed by mTOR, mLST8 and Raptor (mTORC1) (20). In turn, mTORC1 integrates signaling evoked by nutrients and growth factors to regulate mRNA translation initiation (17). Activated mTORC1 phosphorylates S6K1 and the translation inhibitory pro-

*To whom correspondence should be addressed. Tel: +39 0636733576; Email: mariapaola.paronetto@uniroma4.it
†These authors contributed equally to this work as first authors.

tein 4E-BP1, causing its release from the translation initiation factor eIF-4E and promoting cap-dependent translation (20). Dysregulation of several components of this pathway, such as AKT, 4E-BP1, S6K1 and eIF-4G, is associated with poor survival in rhabdomyosarcoma, a pediatric sarcoma of soft tissues displaying very similar histology and therapeutic treatment with ES (21). Moreover, IGF-IR signaling is commonly activated in musculoskeletal sarcomas, including ES, osteosarcoma and rhabdomyosarcoma, and leads to aberrant activation of both the PI3K/AKT/mTOR and MAPK signaling cascades (22). Thus, given its implication in cancer cell proliferation, the PI3K/AKT/mTOR pathway is generally considered a suitable therapeutic target for ES as well as for other human cancers (23). However, although the mTOR inhibitor rapamycin and its derivatives are currently being evaluated in clinical trials (24,25), resistance to these drugs is frequently observed and involves, at least in part, cross-talk with IGF-IR signaling and PI3K/AKT activation (26). Some patients treated with rapamycin analogues showed an increase in AKT phosphorylation/activation in tumor cells and this effect is thought to underlie the limited clinical progress of these drugs (27). Dual inhibition of both PI3K and mTOR catalytic activity has been proposed to counteract acquired resistance to mTOR inhibitors (28–30) and might represent a valuable therapeutic strategy also for the treatment of ES and other sarcomas.

Elucidation of the gene expression changes occurring in response to therapeutic treatments of ES cells could uncover promising candidates for diagnostic and therapeutic applications. Alternative splicing (AS) of pre-mRNAs represents an important layer of gene expression that is often altered in human cancer cells (31). AS allows production of multiple mRNA isoforms from a single gene, thus amplifying proteomic and functional diversity in metazoans. Splicing insures removal of non-coding sequences (introns) from the pre-mRNA and ligation of the exons (32). This process is driven by the spliceosome, a large macromolecular complex composed of five small nuclear ribonucleoproteins (snRNPs) and over 200 auxiliary proteins (32). Additional regulatory factors modulate splice site recognition, including RNA-binding proteins (RBPs) that are recruited to specific sequence elements present in exons or in introns (33–35). Interestingly, AS often regulates subsets of genes that are not co-regulated at the transcriptional level (36), like several apoptotic genes (*BCL2L1, APAF1* and *FAS*), genes involved in cell adhesion (i.e. fibronectin) and genes involved in cell metabolism, like *PKM1*, yielding splice variants that display different functions (31,37–39).

In this study, we analyzed the modulation of the ES cell transcriptome in response to dual inhibition of PI3K and mTOR kinases. Splicing-sensitive exon junction microarray analysis identified the gene expression network regulated both at transcriptional and post-transcriptional levels. Notably, the RBP hnRNPM was strongly up-regulated both at mRNA and protein level upon inhibition of the PI3K/AKT/mTOR pathway, thus driving a specific co-transcriptional program. Impairment of hnRNPM activation by RNA interference abolished the hnRNPM-induced splicing program. Moreover, up-regulation of hnRNPM correlated with poor prognosis in sarcoma patients and its knockdown in ES cells significantly reduced clonogenicity. These findings suggest that hnRNPM expression is a valuable prognostic factor in ES and that inhibition of its activity could represent a suitable therapeutic target to increase susceptibility of ES cells to treatment with PI3K/AKT/mTOR inhibitors.

MATERIALS AND METHODS

Cell cultures, transfections and extract preparation

Human TC71, LAP35 and SK-N-MC cells were maintained in Iscove's modified Dulbecco's medium (IMDM, GIBCO), supplemented with 10% fetal bovine serum. Transfection of TC71 cell line was performed using RNAimax reagent (Invitrogen) according to manufacter's instructions. TC71 cell line was trasfected with control siRNA (Sigma Aldrich) and siRNA for hnRNPM (SantaCruz Biotechnology) at the final concentration of 30 nM. BEZ235 was purchased from EMD Chemical Inc./Calbiochem. Inhibitors were dissolved in dimethyl sulfoxide and aliquots were stored at -20°C. Stock solutions were diluted to the final concentrations in growth medium just before use. At the end of the incubation, cells were washed twice with ice-cold phosphate buffered saline (PBS), resuspended in RIPA lysis buffer [150 mM NaCl, 50 mM Tris–HCl pH 7.5, 2 mM EDTA, 0,1% in sodium dodecyl sulfate (SDS), 0,5% sodium deoxycolate, 1 mM dithiothreitol, 0,5 mM Na-ortovanadate, 10 mM B-glycerolphosphate, 10 mM sodium fluoride, 1% NP-40 and Protease-Inhibitor Cocktail (Sigma-Aldrich)] and kept on ice for 10 min. Soluble protein extracts were separated by centrifugation at 12 000 rpm for 10 min and diluted in sodium dodecyl sulfate (SDS) sample buffer.

Cell culture and *in vitro* treatments

TC71 cells were plated into in 60 mm dishes in Iscove's modified Dulbecco's medium plus 10% fetal bovine serum. After 24 h, various concentrations of BEZ235 (30 nM to 3 μM), wortmannin (10 μM) and LY (10 μM) were added and cells were exposed up to 16 h. Cells were also treated with DMSO-containing medium as a control.

Human Affymetrix Exon-Junction Arrays

RNA from three biological replicates of control or BEZ235 treated TC71 cells was isolated and DNase digested using Quiagen RNeasy kit. Its quality was determined by RNA integrity (RIN) number analysis using Bioanalyzer, and samples with a RIN $>$ 9.5 were used following the Affymetrix labelling procedure. Total RNA was then hybridized to Human Affymetrix Exon-Junction Array (HTA2). Detailed description can be found in the Supplemental Information. Results are considered statistically significant for uncorrected *P*-values $\leq$0.05 and fold-changes $\geq$1.5.

Bioinformatic analysis

Analysis of consensus motifs enriched in introns surrounding regulated exons was performed as previously described

(40). The first 9 and last 30 nucleotides, which contain the conserved 3′ and 5′ splice sites, were excluded from the analysis. 432 'simple exon' were selected from the originally identified 577 cassette exons by excluding the 'multiple exons'. Four groups of sequences were generated, containing: group 1, first 241 nt of upstream introns; group 2, last 220 nt of upstream introns; group 3, first 241 nt of downstream introns; group 4, last 220 nucleotides of downstream introns. Next, pentamer enrichment analysis was performed for each set to obtain the observed number of pentamers within intron sequences, and then computing pentamer number according to a first order Markov model.

Pentamer enrichment was calculated using the binomial distribution and all *P*-values were subjected to a false discovery rate (Benjamini–Hochberg, FDR > 0.05). To assess conservation, UCSC 46-way multiple alignments was used to detect conserved pentamers within six mammalian genomes, mouse, human, dog, marmoset, horse and cow (*m4, hg19, canFam2, calJac1, equCab2* and *bosTau4*, respectively). A pentamer with at least five times sequence coverage was considered as *conserved*. A conservation rate was calculated as fraction of aligned and conserved pentamer occurrences.

Functional gene annotation clustering for BEZ235 predicted regulated genes was performed by using DAVID Bioinformatic Database (https://david.ncifcrf.gov/summary.jsp).

CLIP assays

CLIP assays were performed as previously described (5). In brief, TC71 cells were irradiated once with 400 mJ/cm^2 in a Stratalinker 2400 at 254 nm. Detailed description can be found in the Supplemental Information.

RESULTS

BEZ235 efficiently affects growth of Ewing sarcoma cells

To investigate the transcriptional response of ES cells to inhibition of the PI3K/AKT/mTOR pathway, we tested the activity of three PI3K inhibitors in the TC71 cell line: the commonly used wortmannin and LY294002, and BEZ235, a synthetic imidazoquinoline targeting both PI3K and mTOR kinase activity by competing with their ATP-binding site (41). The TC71 cell line was established from a 22-year-old man with metastatic ES that arose in the humerus; it was derived from a biopsy of recurrent tumor at the primary site and it carries the characteristic chromosomal translocation t(11;22)(q24;q12) leading EWS-FLI-1 fusion. Since this translocation has the highest frequency in ES (2), TC71 cells were chosen as model for this study. Western blot analyses of the phosphorylation status of AKT (phAKT) and of the mTORC1 target 4E-BP1 (slow mobility bands) indicated that BEZ235 was the most effective inhibitor of the pathway (Supplementary Figure S1A). Accordingly, BEZ235 was also the most potent inhibitor of the clonogenic activity of ES cells (Supplementary Figure S1B). Importantly, the cytostatic activity of BEZ235 was not due to induction of cell death, as measured by propidium iodide (PI) staining and flow cytometry, whereas wortmannin treatment strongly induced apoptosis (Supplementary Figure S1C). A dose-response experiment indicated that BEZ235 significantly reduced TC71 cell clonogenic potential at 30 nM, and almost completely abolished it at 300 nM and 3 μM (Figure 1A). PI staining showed that viability was only slightly affected by the treatment with 30 and 300 nM of BEZ235, while 3 μM BEZ235 elicited strong cytotoxic effects (Figure 1B). Moreover, western blot analysis showed that PARP cleavage occurred only at highest concentration of the drug (Figure 1C). We concluded that 300 nM BEZ235 elicits cytostatic effects and mild or no apoptotic effect. To monitor the effect of BEZ235 on cell cycle progression, we performed a BrdU pulse in the last 30 min of treatment with 300 nM BEZ235, or the vehicle DMSO alone, for 16 h. BEZ235 induced a significant increase in G1-phase (41% versus 64%) cells and reduction in S-phase (43% versus 20%) cells (Figure 1D and E). Collectively, these experiments indicate that BEZ235 is the most suitable drug for analysis of the transcriptional response of ES cells to inhibition of the PI3K/AKT/mTOR pathway in the absence of secondary cytotoxic effects.

Inhibition of the PI3K/AKT/mTOR pathway leads to global changes in the transcriptome of Ewing sarcoma cells

To depict the genome-wide picture of transcriptional and post-transcriptional changes in gene expression induced by inhibition of the PI3K/AKT/mTOR pathway, we treated TC71 cells with 300 nM BEZ235 for 16 h, a concentration sufficient to inhibit cell growth without inducing cell death (Figure 1). Under these conditions, AKT, rpS6, 4E-BP1 and mTOR phosphorylation was almost completely inhibited (Figure 2A). RNA from three biological replicates of control (DMSO) or BEZ235-treated cells was hybridized with Affymetrix Human Exon Junction Arrays (HTA2). Bioinformatics analyses highlighted extensive reprogramming of the TC71 transcriptome upon inhibition of the PI3K/AKT/mTOR pathway (Figure 2B), with 3541 genes that were modulated at the expression level (1501 up-regulated and 2040 downregulated, average fold change of |2.1|; Supplementary Table S1). Gene ontology (GO) analysis revealed functional categories related to cell cycle (fold enrichment 3.4, *P* value = 2.90E–12), cancer (fold enrichment 2, *P* value = 2.20E–2) and p53 signaling pathways (fold enrichment 3.7, *P* value = 3.60E–8) being enriched in the down-regulated genes (Supplementary Figure S2A and B), whereas spliceosome, non-homologous end-joining and metabolic categories were enriched among the up-regulated genes (1.9-fold enrichment, *P* value = 2.20E–2; Supplementary Figure S2A and B). This result suggested a specific activation of splicing as feedback response of ES cells to PI3K/AKT/mTOR inhibition.

In keeping with this observation, we identified 1440 differentially regulated AS events in 918 genes (Figure 2C, Supplementary Table S2). Remarkably, there was a highly significant overlap (*P* = 7.29E–27) between genes affected at gene expression and splicing level (391, 42.6%; Figure 2C). GO analysis revealed that splicing regulated genes are involved in cell-cell interactions, splicing, protein metabolism and cancer-related signaling pathways (Figure 2D). BEZ235 treatment exerted a significantly higher impact on cassette exon events (577 regulated exon cas-

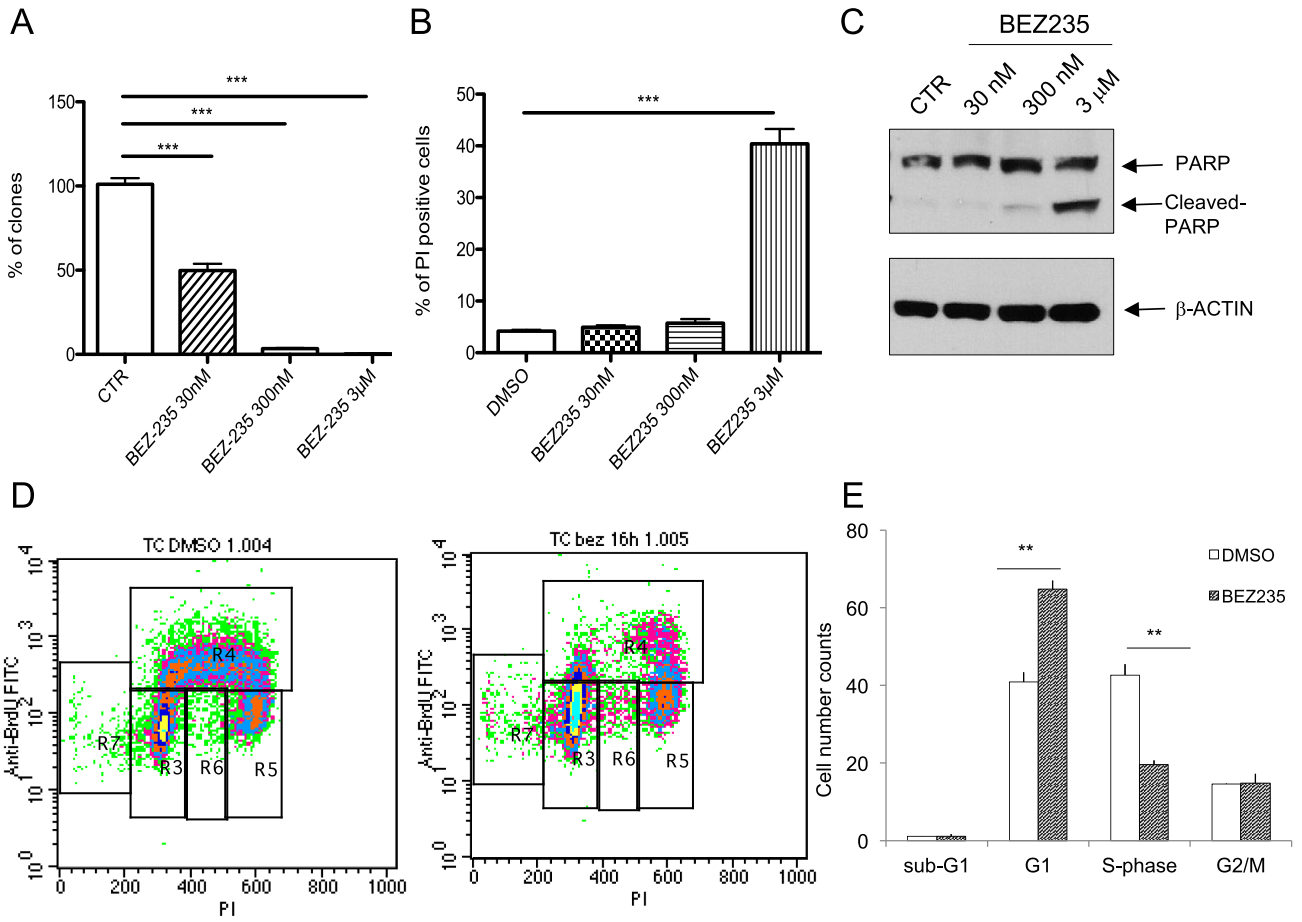

Figure 1. BEZ235 affects Ewing sarcoma cell growth. (**A**) Colony assay carried out on TC71 cells upon treatment with different concentration of BEZ235 (30 nM, 300 nM, 3 μM). Histograms represent percentage of colony numbers ($n = 3$; mean ± S.D.). Statistical analysis was performed by Student's *t*-test: $*P < 0.05$, $**P < 0.01$, $***P < 0.001$ for DMSO versus BEZ235 treatment. (**B**) Propidium Iodide (PI) viability assay; the decrease in viability was expressed as relative percentage of dead cells in treated versus control cells. Statistical analysis was performed by Student's *t*-test: $*P < 0.05$, $**P < 0.01$, $***P < 0.001$ for DMSO versus BEZ235 treatment. (**C**) Western blot analysis of TC71 cells after treatment with different doses of BEZ235 (30 nM, 300 nM, 3 μM). The un-cleaved and cleaved form of PARP-1 protein were detected; β-actin was used as loading control. (**D** and **E**) Cell cycle analysis of TC71 treated with 300 nM of BEZ235 performed by BrdU and PI staining. On the left D), representative images of cytofluorimetric plots. On the right E), histograms represent the percentage of cells in different stages of the cell cycle (sub-G1, S, G1 and G2/M) (mean ± S.D.). The experiments were performed at least three times; statistical analysis was performed by unpaired Student's *t*-test ($*P < 0.05$; $**P < 0.01$; $***P < 0.001$).

sette events; $P = 5.74E{-}128$) in comparison with what expected from the array design (Figure 2E, Supplementary Figure S2C). Sixteen randomly selected AS events were validated by RT-PCR analysis (i.e. cassette exons in *BPTF, SPTAN1, NFAT5, SETD4, PAX6, NFYC, CASP2, SRRM1, BCLAF1, ZDHHC16, NUMB, HNRNPA2B1, AKAP13* and *SH3BGRL* genes and the alternative terminal exon in *CFLAR* gene; Figure 3 and Supplementary Figure S3). Furthermore, choice of mutually exclusive exons in *FYN* was also validated by quantitative RT-PCR (qPCR; Figure 3). These results confirm the reliability of the array and bioinformatics analyses and uncover an extensive splicing program set in motion by PI3K/AKT/mTOR pathway inhibition in ES cells.

Identification of consensus motifs enriched in exons regulated by the PI3K/AKT/mTOR pathway in Ewing sarcoma cells

Regulation of AS is generally achieved by the interaction of trans-acting proteins with *cis*-acting sequences (42). Regulatory sequences can be located both in exons and flanking introns, and are classified as enhancers or silencers if they promote or repress, respectively, exon recognition (42–44). Generally, enhancer sequences are recognized by members of the Serine-Arginine (SR) protein family, while the heterogeneous ribonucleoproteins (hnRNPs) interact with splicing silencers (43). The combinatorial control achieved by these splicing factors with the multiple regulatory cis-acting elements allows extreme accuracy and flexibility of AS regulation (42,45,46). To investigate the specific splicing signature elicited by BEZ235 treatment, we isolated 432 regulated cassette exons and searched for consensus motifs enriched in the intronic sequences surrounding the regulated exons. The first 9 and last 30 nucleotides, which con-

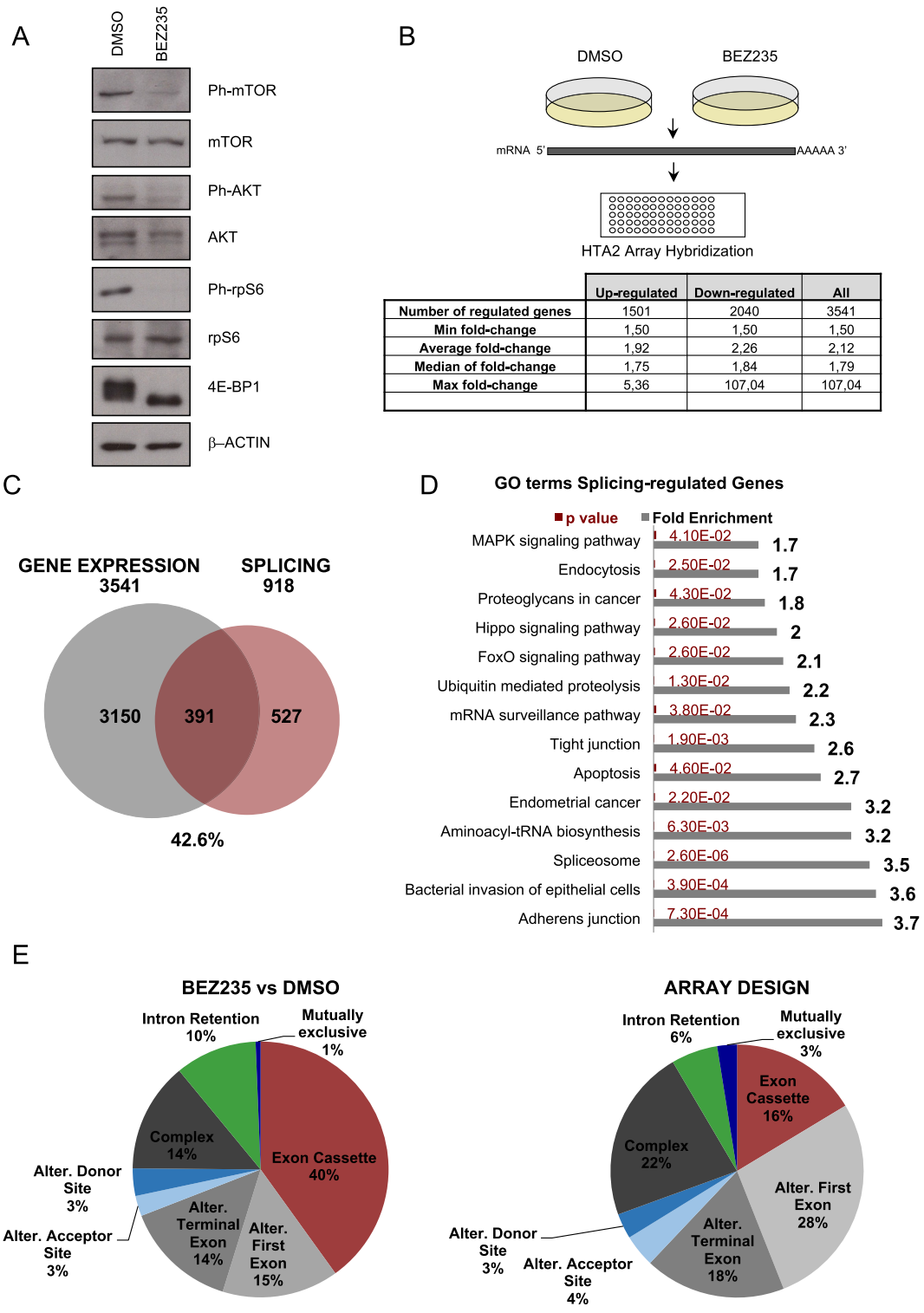

	Up-regulated	Down-regulated	All
Number of regulated genes	1501	2040	3541
Min fold-change	1,50	1,50	1,50
Average fold-change	1,92	2,26	2,12
Median of fold-change	1,75	1,84	1,79
Max fold-change	5,36	107,04	107,04

Figure 2. Inhibition of the PI3K/AKT/mTOR pathway leads to global changes in the transcriptome of ES cells. (**A**) Western blot analysis of ph-mTOR, mTOR, ph-AKT, AKT, ph-rpS6, rpS6 and 4E-BP1 to evaluate the activity of PI3K/AKT/mTOR pathway. β-ACTIN was used as loading control. (**B**) Schematic representation of HTA2 Hybridization Array experiment. Table summarizes changes of gene expression between TC71 cells treated with DMSO and BEZ235. (**C**) Venn Diagrams show genes regulated at the expression level, splicing, or both upon BEZ235 treatment. (**D**) Gene ontology functional annotation clustering of GO terms regulated at splicing levels by BEZ235 treatment. Histograms represent the overall enrichment score for the group based on the EASE score (a modified Fisher Exact *P*-value), set to 0.05 for each term. The higher, the more enriched. The Group Enrichment Score is used to rank the biological significance of each term. Terms are listed for enrichment score ≥1.5. In red is reported the *P*-value and in black the fold enrichment for each GO term. (**E**) Pie charts show the comparison of type of alternative splicing event in BEZ235 treated cells (left) versus the array design (right). For the statistical analysis see Supplementary Figure S2C.

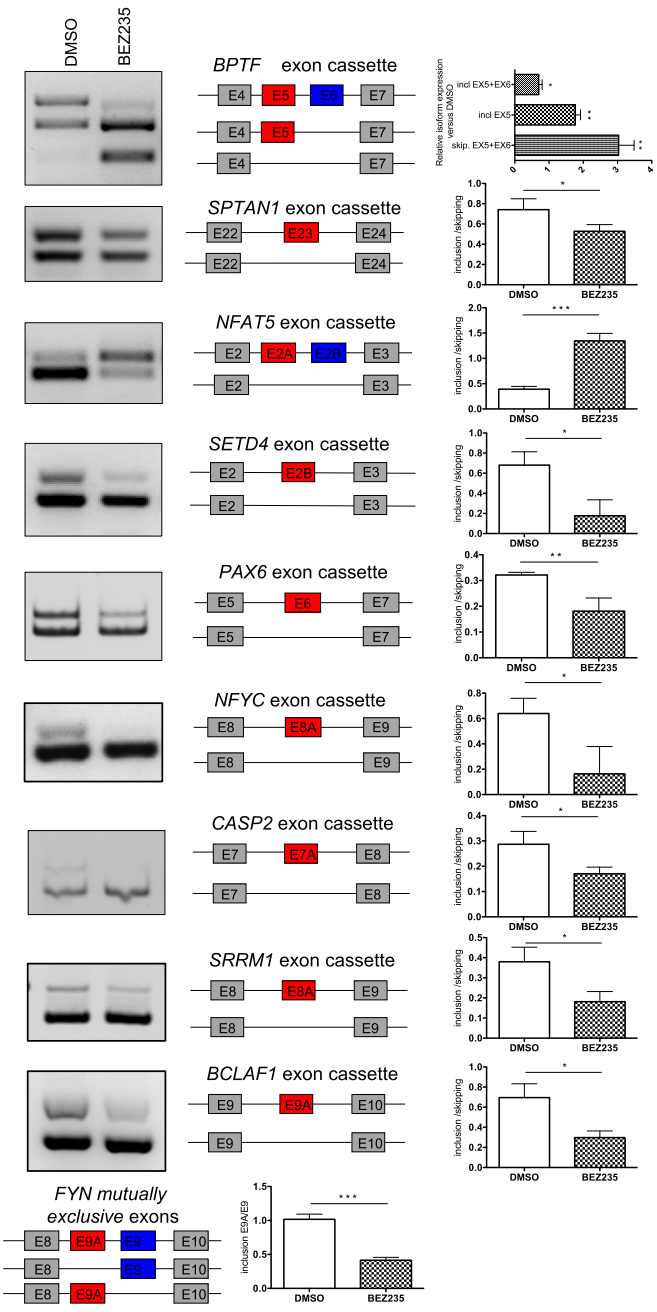

Figure 3. Validation of splicing events regulated by BEZ235 treatment. Representative images of RT-PCR analyses for the indicated alternative splicing events differentially regulated between DMSO and BEZ235 300 nM 16h-treatment. See also Supplementary Figure S3. RT-PCR of exon cassette events (in red in the scheme) affected by 300 nM BEZ235 treatment. RT-PCR was performed using primers in constitutive exons (in gray in the scheme) of *BPTF, SPTAN1, NFAT5, SETD4, PAX6, NFYC, CASP2* and *BCLAF1* genes. For each event, representative gel images, scheme of the regulated event and densitometric analysis of at least three experiments were reported. For each experiment DNAse digestion and no-RT control have been performed. The graphs show the densitometric analysis of the ratio between isoforms with included and skipped exons (mean ± S.D.). Mutually exclusive exons in *FYN* pre-mRNA were validated by quantitative (q)-PCR. The graph shows the ratio between fold enrichment of exon 9A and 9 in BEZ235 vs DMSO treated cells (mean ± S.D.). Statistical analysis was performed by Student's *t*-test student (**P* <0.05; ***P* < 0.01; ****P* < 0.001).

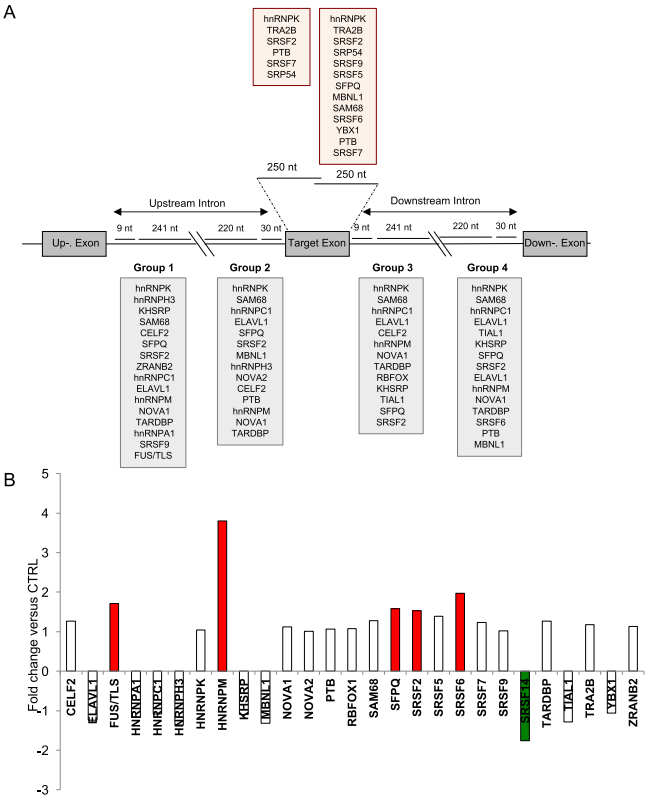

Figure 4. Specific *cis*-Acting Elements feature BEZ235 signature. (**A**) Schematic representation of predicted RBPs binding *cis*-acting elements surrounding the regulated cassette exons. Regions were subdivided in first 241 nt (Group1) and last 220 nt (Group 2) of upstream introns, first 241 nt (Group 3) and last 220 nucleotides (Group 4) of downstream introns. The scheme also reports pentamer enrichments in the first and last 250 nucleotides within regulated exons. For the conserved and enriched pentamers see also Supplementary Figure S4 and Tables S3–S6. (**B**) Expression profile of the potential regulators (RBPs) of cis-acting elements in (A) from the array analysis. Bar graphs represent gene expression fold changes versus DMSO. In red are represented RBPs upregulated at least 1.5 versus DMSO. In green are represented RBPs downregulated at least 1.5 versus DMSO. See also Supplementary Figure S5.

tain the conserved 3′ and 5′ splice sites, were excluded from the analysis. Four groups of sequences were generated (Figure 4A), containing: group 1, first 241 nt of upstream introns; group 2, last 220 nt of upstream introns; group 3, first 241 nt of downstream introns; group 4, last 220 nucleotides of downstream introns. Pentamer enrichment analysis was performed within intron sequences and then computed according to a first order Markov model. Moreover, the conservation rate was calculated as fraction of aligned and conserved pentamer occurences (see Materials and Methods for details). We identified 35 significantly enriched pentamers in the first group, 21 in the second group, 27 in the third group and 31 in the fourth group (*P*-value < 0.05; Supplementary Figure S4A, Table S3). Moreover, we found 18 conserved pentamers in the first group, 10 in the second, 198 in the third and 18 in the fourth group (CR <0.3; Supplementary Figure S4B, Table S4). The same analysis was performed for exonic sequences, dividing them in two groups, one for the first 250 nt and the second for the last 250 nt. We identified

18 enriched pentamers in the first group and 30 in the second group (P-value < 0.05; Supplementary Figure S4C; Table S5). Moreover, we found 54 conserved pentamers in the first group and 52 in the second (CR < 0.3 (Supplementary Figure S4D; Table S6). This analysis identified hnRNPK consensus motif as the most significantly enriched in each group of the BEZ235-regulated cassette exons (Figure 4A). Notably, motifs for hnRNPK, SRSF2 and SAM68 were enriched in all exon and intron sequences analyzed, whereas hnRNPM and hnRNPC1 motifs were enriched specifically in all groups of intronic sequences (Figure 4A).

Next, we searched for RBPs whose expression was modulated upon BEZ235 treatment. *HNRNPM* transcript was strongly upregulated, whereas *SRSF1*, *SRSF2*, *SRSF3* and *SRSF6* mRNAs were induced at lower levels and *SRSF14* was downregulated (Figure 4B, Supplementary Figure S5A). We also found that transcripts encoding several helicases were affected by the treatment; in particular, *DDX1, DDX17*, *DDX23, DDX46* and *DHX9* genes were up-regulated upon inhibition of the PI3K/AKT/mTOR pathway (Supplementary Figure S5A). In the case of *DHX9* the up-regulation of the transcript is likely due, at least in part, to the significant down-regulation of the alternative exon 6A (Fold Change 3.12; P-value 1.10E–03; Supplementary Table S2), that drives the *DHX9* transcript to nonsense mediated RNA decay (47). Importantly, changes in *SRSF1*, *SRSF2*, *HNRNPM*, *FUS* and *DHX9* expression were all validated by qPCR analysis (Figures 4B, 5A and Supplementary Figure S5B). *QKI*, which was not affected in the array prediction, was used as negative control of the treatment.

hnRNPM expression and subnuclear localization are regulated by inhibition of the PI3K/AKT/mTOR pathway

HnRNPM was the most up-regulated RBP mRNA by BEZ235 treatment (Figure 4B) and this increase resulted in concomitant up-regulation of the protein (Figure 5B). Cell fractionation analyses revealed that the majority of hnRNPM protein was associated with chromatin and other high-molecular-weight (HMW) material, with less than 35% of the protein present in the soluble nuclear fraction where spliceosomal proteins were found (i.e. U1C, U2AF65 and U170K; Figure 5C). However, treatment with BEZ235 augmented the fraction of hnRNPM protein cosedimenting with U1C, U170K and U2AF65 in the soluble nucleoplasm (∼60%), consistent with its engagement in spliceosomal activity. This shift in subnuclear localization was not a general feature of splicing factors. Indeed, while hnRNP C1/C2 was also significantly translocated in the nucleoplasm (from ∼10% of DMSO treated cells to ∼40% in BEZ235 condition), MATRIN3 and hnRNPK localization, like that of U1C, U170K and UAF65, was predominantly nucleoplasmic and not affected by the treatment, (Figure 5C). Furthermore, we found that co-immunoprecipitation of hnRNPM with the spliceosomal protein U170K, a core component of the U1 snRNP, was robustly increased upon BEZ235 treatment (2.5 times; Figure 5D). These findings indicate that inhibition of the PI3K/AKT/mTOR pathway in ES cells promotes expression and functional recruitment of hnRNPM to the splicing machinery, thus possibly affecting the splicing response to this stress.

hnRNPM regulates a subset of the PI3K/AKT/mTOR-sensitive splicing events in ES cells

Among the 14 putative hnRNPM consensus motifs previously identified by CLIP-seq experiments (48), only UGUGU displayed a significant enrichment in both distal (groups 1 and 4) and proximal (groups 2 and 3) intronic sequences flanking the BEZ235-regulated exons (Figure 4A; Supplementary Tables S3 and S7). To test if these exons were regulated by hnRNPM, we silenced it by RNA interference (RNAi) in TC71 cells (Figure 6A and B) and monitored the outcome on AS of randomly chosen regulated exons (Figure 6C and D). Remarkably, the influence on BEZ235-induced AS depended on the position of the hnRNPM binding site. Cassette exons containing proximal hnRNPM consensus motifs (last 220 nt upstream or first 241 nt downstream; group 2 and 3 introns) were completely reverted by hnRNPM silencing (Figure 6C). In all cases tested, hnRNPM promoted skipping of the target exon, regardless of whether its binding site was upstream, within or downstream of the exon. Moreover, comparison of all up- and down-regulated exons between groups 2 and 3 revealed no significant difference in regulation (Fisher's test $P = 0.75$; 63 up- and 64 down-regulated exons in group 2 and 62 up- and 84 down-regulated exons in group 3). On the contrary, cassette exons flanked by distal intronic consensus motifs (first 241 nt upstream or last 220 nt downstream; group 1 and 4) were not affected by hnRNPM knockdown (Figure 6D). To test whether intron length was a determinant in hnRNPM regulation, introns were classified in four group: <1000 bp; between 1000 and 5000 bp; between 5000 and 10 000 bp; ≥10 000 bp). We found that hnRNPM regulated exons are preferentially flanked by relatively short introns (<5000 bp in all four groups). However, no substantial difference in intron length was found between groups 1–4 and 2–3, suggesting that the splicing effect of hnRNPM requires proximal binding to the exon regardless of the length of surrounding introns (Supplementary Figure S6A). These results suggest a positional effect of hnRNPM on splicing regulation that requires its binding proximal to the exon, regardless of the length of surrounding introns.

To validate whether the effect of hnRNPM on splicing was due to direct binding near the exon, we performed cross-linked and immunoprecipitation experiments (CLIP). In line with the hypothesis, we detected direct *in vivo* binding of hnRNPM to the predicted regions of regulated exons, while regions randomly chosen nearby cross-link sites were not bound (Figure 6E). Importantly, binding of hnRNPM to *PAX6*, *SPTAN1, SETD4* pre-mRNAs (groups 2 and 3) was increased upon BEZ235 treatment, while that to group 1 *NFAT5* pre-mRNA was decreased (Figure 6F). This results indicate a direct effect of hnRNPM on splicing of target exons.

Some of the BEZ235-dependent hnRNPM-regulated events were also identified by other laboratories using iCLIP and RNAseq experiments (48–50). Although these datasets were obtained from completely different tissues, like brain (49) and breast cancer (48), several genes contain-

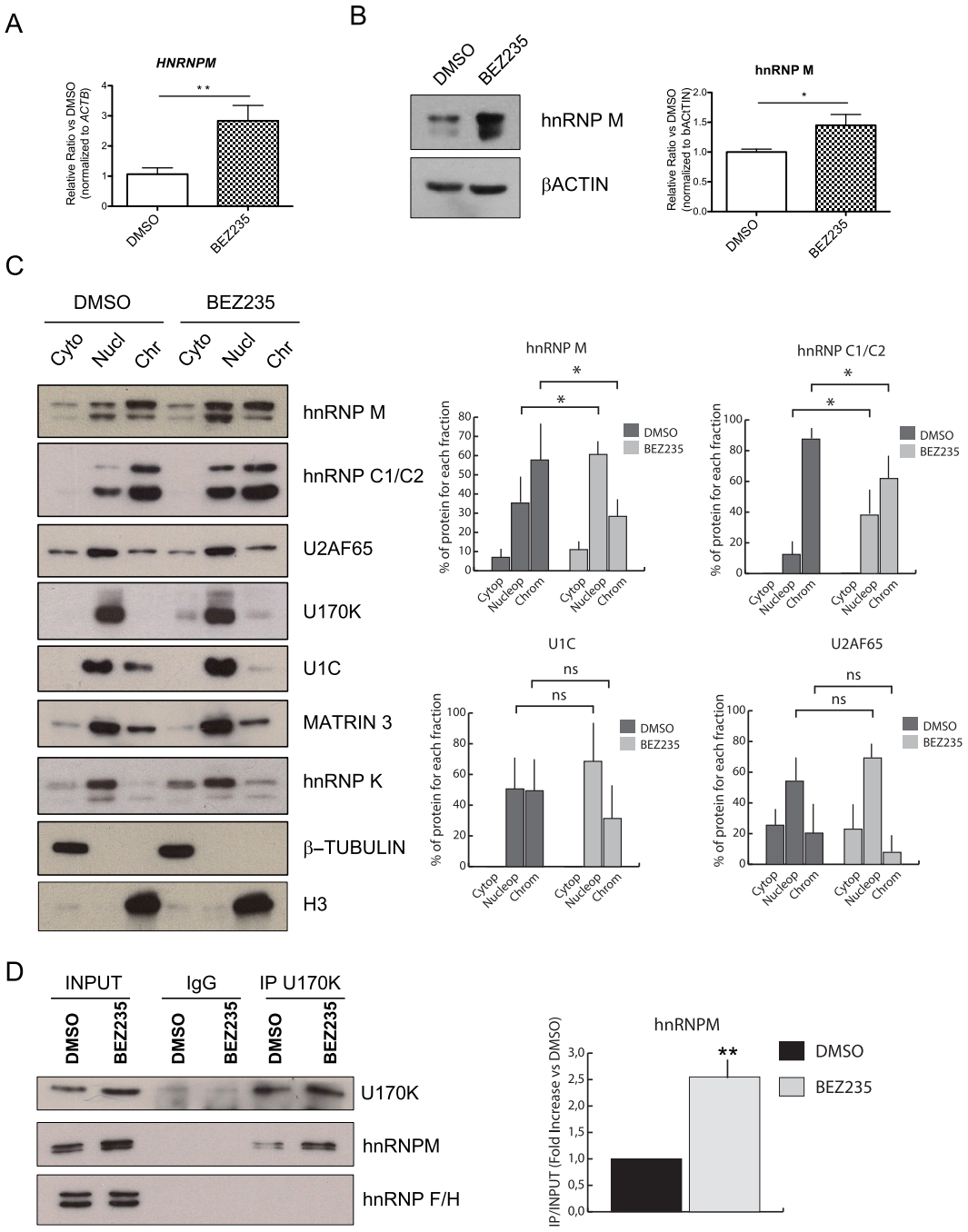

Figure 5. hnRNPM upregulation upon BEZ235 treatment and interaction with U170K in the Triton soluble nuclear fraction. (**A**) RT-qPCR analysis of *HNRNPM* in TC71 Ewing sarcoma cells after 16-h treatment with 300 nM BEZ235 or the vehicle alone. Histograms represent *HNRNPM* expression (mean ± S.D.) in three independent experiments. Statistical analysis was performed by Student's *t*-test (***P* <0.01). (**B**) Western blot analysis of hnRNPM in TC71 cells treated for 16 h with either DMSO or BEZ235 300 nM. β-Actin was used as loading control. Histograms represent densitometric analysis of hnRNPM expression (mean ± S.D.). HnRNPM is represented by a group of four different protein isoforms arising from the same gene *locus*, known as hnRNP M1, M2, M3 and M4 (64). The upper band corresponds to hnRNP M3 and M4, while the lower band corresponds to hnRNP M1 and M2. (**C**) Cytosolic (Cyto), nuclear soluble (Nucl) and nuclear insoluble chromatin-associated (Chr) fractions (obtained as previously reported (72)) of TC71 cells were analysed upon BEZ235 treatment by western blot, using antibodies against hnRNPM and the indicated splicing factors. Histone H3 and β-Tubulin were evaluated, respectively, as nuclear chromatin associated fraction and cytosolic markers. Western blot analysis of hnRNPM, hnRNPC1/C2, U2AF65, U1C, U170K, MATRIN3 and hnRNPK from the sub-cellular fractionation of TC71 treated with DMSO and 300 nM BEZ235 for 16 h. Histograms show the percentage of hnRNPM, hnRNPC1/C2, U1C and U2AF65 co-sedimenting in each fraction (mean ± S.D.). The experiments were performed at least three times; statistical analysis was performed by Student's *t*-test (**P* <0.05). (**D**) Western blot analysis of U170K and hnRNPM after immunoprecipitation (IP) of endogenous proteins from TC71 nuclear extracts with anti-U170K or control rabbit IgGs. On the right, bars represent the percentage of input of hnRNPM associated to U170K in control (DMSO) or BEZ235 immunoprecipitates. The experiments were performed at least three times; statistical analysis was performed by Student's *t*-test (***P* <0.01).

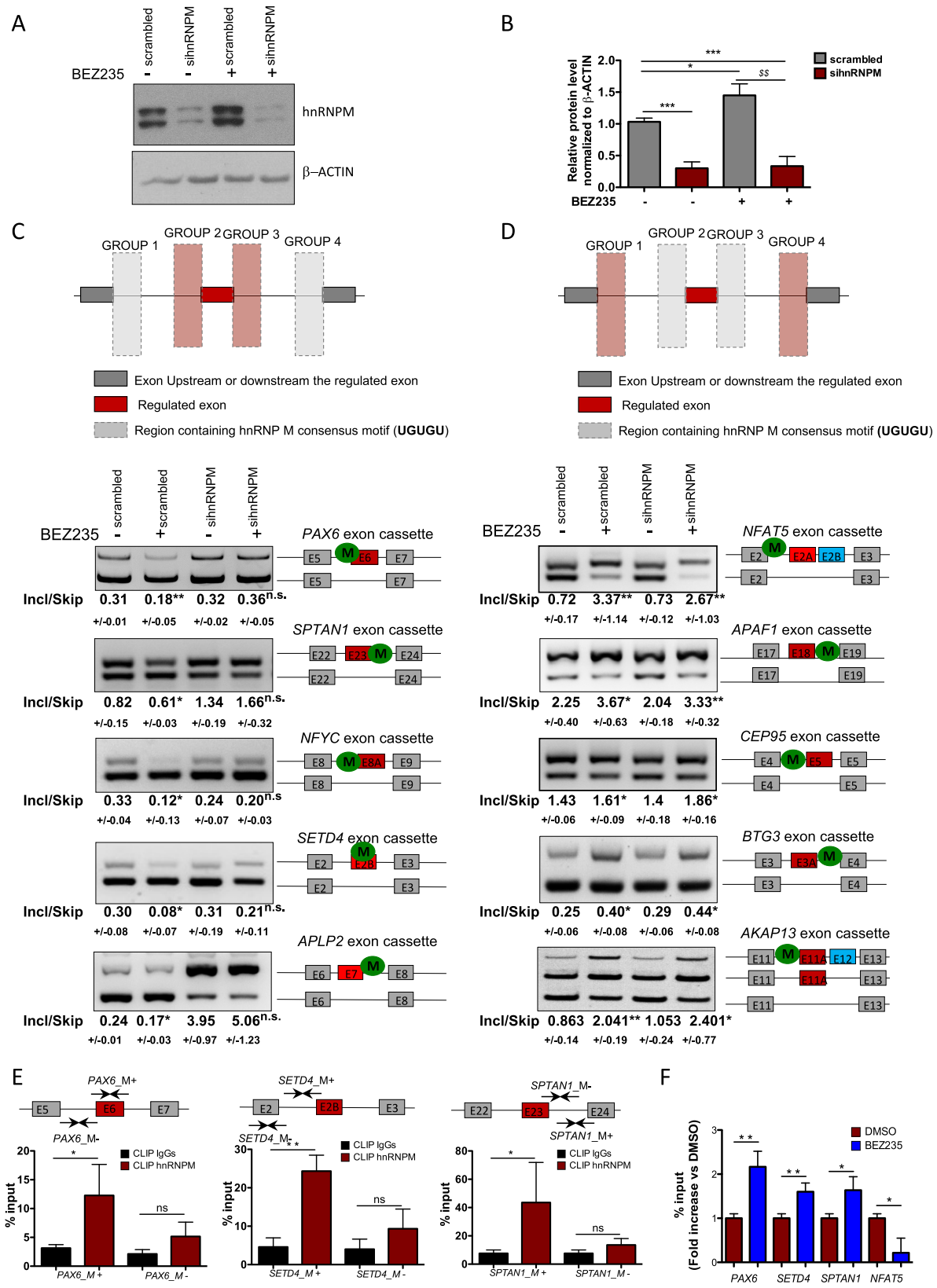

Figure 6. hnRNPM regulates BEZ235 splicing signature. (**A**) Western Blot analysis of hnRNPM in TC71 cells transfected with either scrambled or siHNRNPM oligonucleotides, treated with DMSO or BEZ235 300 nM for 16 h. β-Actin was used as loading control. (**B**) Histograms represent the relative protein level for scrambled (gray bars) or siHNRNPM (red bars) normalized to β-actin from three independent experiments. Statistical analysis was

ing regulated exons seem to be conserved (26 out of 213 in one case and 5 in the second case). Likewise, only 25 genes are conserved between the two datasets (48–50; Supplementary Figure S6B). Thus, hnRNPM splicing regulation appears to be context-dependent.

These experiments demonstrate that modulation of hnRNPM expression contributes to the molecular response of ES cells to inhibition of the PI3K/AKT/mTOR pathway.

hnRNPM expression is associated with malignancy of ES cells

Gene ontology analysis revealed that hnRNPM regulated genes were involved in p53, FoxO and MAPK signaling pathways, spliceosome and cellular junctions (Supplementary Figure S6C). Since all these functional categories are highly relevant to human cancer, we asked whether the expression levels of hnRNPM affect the sensitivity of ES cells to inhibition of the PI3K/AKT/mTOR pathway. To this end, we used ES cell lines displaying the same (type 2, LAP-35 and TC71) or different (type 1, SKNMC) EWS-FLI-1 chromosomal translocation. HnRNPM is significantly more expressed in LAP35 and TC71 cells than in SKNMC cells (Figure 7A) and its higher expression correlated with higher resistance to BEZ235 treatment (Figure 7B). Moreover, clonogenic assays revealed a significant increase in percentage of LAP35 and TC71 clones in comparison with SKNMC cells upon treatment with 10 nM BEZ235. At a concentration of 30 nM of the drug, TC71 cells were significantly more prone to proliferate and form clones in comparison with the other cell lines (Figure 7C). These experiments suggest that increased expression of hnRNPM promotes resistance of ES cells to inhibition of the PI3K/AKT/mTOR pathway. In line with this hypothesis, hnRNPM depletion significantly increased the sensitivity of ES cells to BEZ235 (Figure 7D and Supplementary Figure S7).

These findings prompted us to query the possible correlation between hnRNPM expression and malignancy by assaying a panel of 260 sarcoma patients from The Cancer Genome Atlas (TCGA). Patients were selected depending on hnRNPM expression levels based on *Z*-score (comparison across all patients). We assayed the data using the threshold $|Z\text{-score}| \geq 0.5$. We identified 159 cases with alteration, and considered patients with hnRNPM *Z*-score ≥ 0.5 as up-regulated and genes with *Z*-score ≤ 0.5 as down-regulated. Kaplan–Meier curves were performed separating patients displaying up-regulation from down-regulation or no alteration in hnRNPM expression. Notably, we found a statistically significant decrease in the overall survival (*P*-value = 1.17E–03) in patients displaying up-regulation of hnRNPM with respect to those characterized by no alteration, while no significant differences were observed in patients with down-regulation of hnRNPM expression (Figure 7E). These results indicate that high hnRNPM expression levels represent a critical prognostic factor for ES malignancy, predicting shorter overall survival of patients.

DISCUSSION

Dysregulation of AS contributes to the pathogenesis of cancer and splice variants expressed by cancer cells can be used to stratify patients according to tumor stage and metastatic potential (31,51). Moreover, splicing regulation and the spliceosome are emerging as suitable targets for anti-cancer therapies (52,53). Therefore, understanding the mechanisms of AS is of critical importance to develop novel therapeutic strategies for the treatment of cancer. One of the hallmarks of malignancy is the acquisition of drug resistance by cancer cells, which strongly impairs therapeutic efficacy. In this study, we have used splicing sensitive arrays to unravel the splicing signature induced upon inhibition of the oncogenic PI3K/AKT/mTOR signaling pathway in ES cells. Our experiments show that inhibition of the PI3K/AKT/mTOR axis induces extensive changes in gene expression and AS. In particular, we found that hnRNPM is specifically up-regulated in response to the treatment and activates a splicing program contributing to drug resistance (Figure 7F), suggesting that modulation of hnRNPM activity could represent a novel therapeutic target for ES treatment. Although our microarray analysis may have missed some transcriptome changes that could be highlighted by more unbiased analyses (i.e. RNA sequencing), it highlights the general response of ES cells to the treatment and indicates that splicing modulation likely contributes to acquired resistance of ES cells to PI3K/mTOR inhibitors.

The PI3K/AKT/mTOR axis is often deregulated in human cancers, including ES, and is considered a valuable therapeutic target for patients. However, despite great preclinical promise, targeted therapies with mTOR inhibitors have demonstrated limited clinical benefit in various cancer types (54–56). This lack of efficacy is largely attributed to acquisition of resistance through up-regulation of feedback responses to treatments. For instance, mTOR inhibition abrogated a negative feedback on IGF1R, resulting in AKT activation both in cancer cell lines and in patient tumors (27,57). Thus, combination therapy ablating

←

performed by Student's *t*-test (*$P < 0.05$; **$P < 0.01$; ***$P < 0.001$; versus scrambled DMSO; $^{\$\$}P < 0.01$ versus scrambled BEZ235). (**C** and **D**) RT-PCR of BEZ235-induced exon cassette events containing intronic hnRNPM consensus motif upstream (Groups 1 and 2) or downstream (Groups 3 and 4) the regulated exon. RT-PCR analysis was performed with RNA extracted from TC71 cells transfected with either scrambled or siHNRNPM oligonucleotides, and treated with DMSO or BEZ235 300 nM for 16 h. Below each lane of the agarose gel, it is reported the densitometric analysis of the ratio between isoforms related to included and skipped exons (mean ± S.D.). The experiments were performed at least three times, statistical analysis was performed by Student's *t*-test ($P < 0.05$ *; $P < 0.01$ **). See also Supplementary Figure S6 and Table S7. **E)** CLIP assay of hnRNPM binding to the predicted target pre-mRNAs. TC71 ES cells were UV-crosslinked and immunoprecipitated with control IgGs or anti-hnRNPM IgGs. The upper panels show a schematic representation of *PAX6, SETD4* and *SPTAN1* splicing events and primers (black arrows) used in the assay. M+ and M– represent amplicons either containing or not hnRNPM consensus motif. The bar graph shows qPCR signals amplified from the CLIP assays expressed as percentage of amplification in the input RNA. IgGs are represented in black, hnRNPM in red. (**F**) CLIP assay of hnRNPM binding to the predicted target pre-mRNAs as in D, performed with TC71 treated either with DMSO or BEZ235 300 nM for 16h, before UV-crosslinking and immunoprecipitation. The bar graph shows qPCR signals amplified from the CLIP assays expressed as percentage of amplification of the input RNA, expressed as BEZ235 (blue bars) fold increase versus DMSO (red bars).

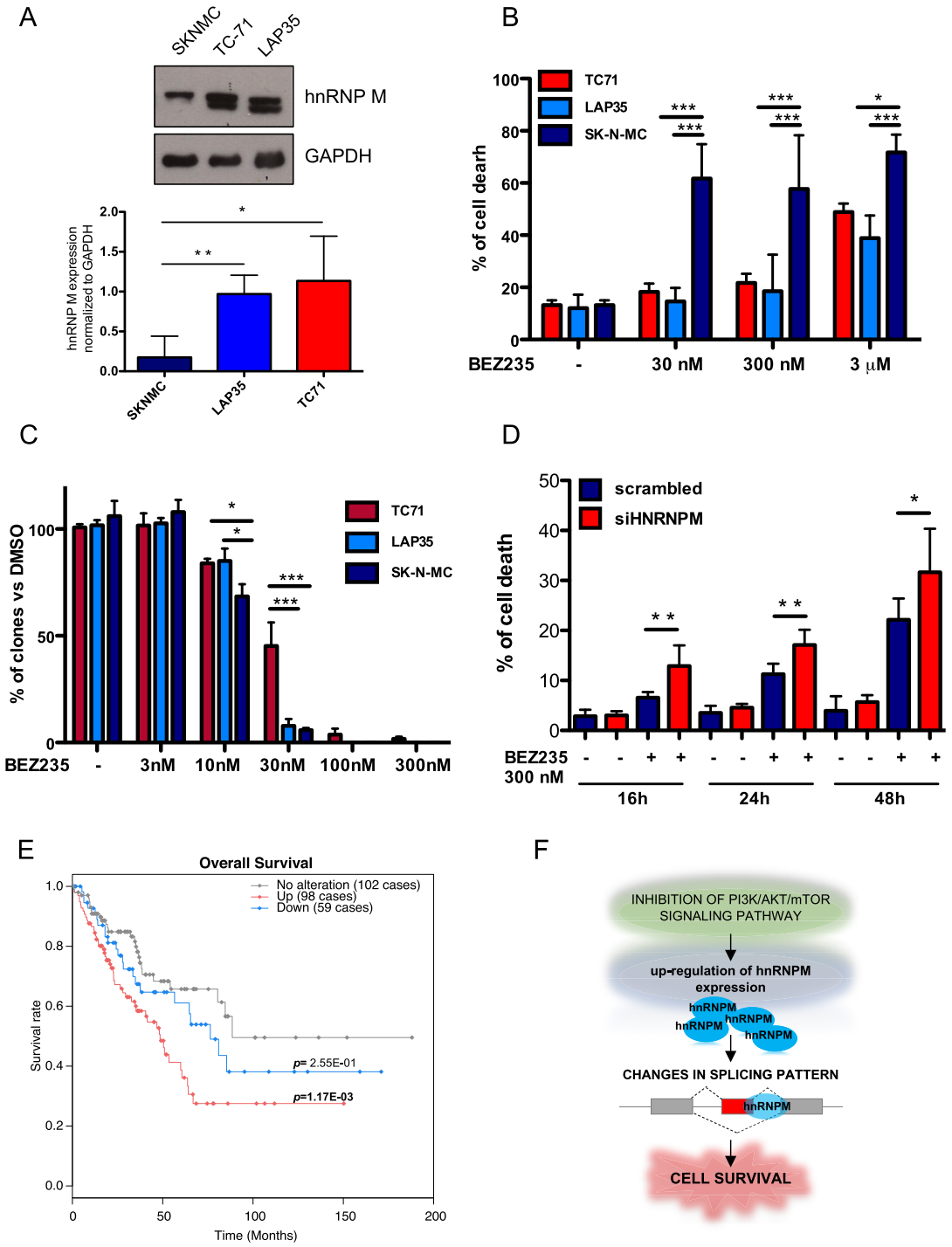

Figure 7. hnRNPM expression is associated with aggressiveness of Ewing sarcoma cells. (**A**) Western Blot analysis of hnRNPM expression in ES cell lines harbouring type 1 (SKMNC, blue bar) and type 2 (LAP35 (cyan bar), TC71 (red bar)) EWS-FLI1 chromosomal translocation. GAPDH was used as loading control. Histogram shows the densitometric analysis of hnRNPM expression (means ± S.D.). Statistical analysis was performed by Student's *t*-test (**P* <0.05; ***P* <0.01). (**B**) Histograms show the percentage of Trypan Blue positive cells upon treatment with different doses of BEZ235 for 16 h (means ± S.D.). Statistical analysis was performed by Student's *t*-test (**P* < 0.05; ***P* < 0.01; ****P* < 0.001). (**C**) Clonogenic assays of SKNMC (blue bars), LAP35 (cyan bars) and TC71 (red bars) Ewing sarcoma cells upon treatment with different doses of BEZ235 or the vehicle alone. Statistical analysis was performed by Student's *t*-test (**P* < 0.05; ***P* < 0.01; ****P* < 0.001). (**D**) Histograms show the percentage of Trypan Blue positive cells upon treatment of scrambled (blue bars) or siHNRNPM (red bars) TC71 cells with 300 nM BEZ235 for 16, 24 and 48 h (means ± S.D.). Statistical analysis was performed by Student's *t*-test (**P* < 0.05; ***P* < 0.01). (**E**) Kaplan–Meier curve of survival rate of sarcoma patients analyzed for hnRNPM expression in The Cancer Genome Atlas (TGCA). The gray line shows the survival rate of patients with no alteration of hnRNPM expression, the red line shows patients with high expression of hnRNPM (*Z*-score ≥ 0.5), blue line shows patients with low expression of hnRNPM. For the two curves, *P*-values versus patients with no-alteration in hnRNPM expression are indicated. (**F**) Model of the accomplishment of a specific splicing program driven by hnRNPM up-regulation upon inhibition of PI3K/AKT/mTOR pathway in Ewing sarcoma cells.

mTOR function and preventing AKT activation may improve the antitumor activity. Second-generation agents, like MLN0128 (Takeda) and the dual inhibitor BEZ235 (Novartis) used in the present study, display inhibitory activity on both mTORC1 and mTORC2 and avoid AKT reactivation (15,58,59), representing valuable alternatives for sarcoma treatment. Clinical trials with these agents are currently being carried out, alone or in combination with other agents (i.e. gemcitabine, irinotecan, cyclophosphamide, etc.; https://clinicaltrials.gov). Pre-clinical studies, in fact, suggest that mTOR inhibitors display synergistic or additive effect with some chemotherapeutic agents. Thus, identification of new potential targets to improve the effect of PI3K/AKT/mTOR inhibition, while preventing acquisition of resistance, could greatly help the efficacy of sarcoma therapy.

Inhibition of the PI3K/AKT/mTOR signaling by BEZ235 elicited strong cytostatic and mild apoptotic effects in ES cells. Such response was accompanied by global modulation of the transcriptome. GO analysis revealed that alternatively processed transcripts are enriched in functional categories involved in cell–cell interactions, splicing and protein metabolism. Bioinformatics analysis of introns surrounding the regulated exons allowed us to identify potential regulators of AS induced by inhibition of the PI3K/AKT/mTOR pathway. We focused on hnRNPM as it was the most upregulated splicing factor and demonstrated that it modulates a subset of BEZ235-regulated splicing events, thus uncovering a role for this RBP in ES malignancy.

HnRNPs modulate AS of pre-mRNAs and affect their fate by influencing the structure and/or by facilitating or hindering the interaction with other pre-mRNA processing factors (60). HnRNPM is an abundant protein that directly influences pre-mRNA splicing by binding GU-rich cis-elements (50,61–63). Proteomic analyses of *in vitro* purified spliceosomes detected hnRNPM in the pre-spliceosomal H-complex (32,64,65). Here, we demonstrate that inhibition of the PI3K/AKT/mTOR pathway affects hnRNPM sub-nuclear localization, promoting its co-fractionation with spliceosomal proteins like U1C, U170K and U2AF65 and its co-immunoprecipitation with U170K (Figure 5C). Thus, by changing sub-nuclear compartment and interactome, hnRNPM may modulate the splicing response to PI3K/AKT/mTOR inhibition. Our results also suggest a positional effect of hnRNPM on splicing and indicate that proximity to the regulated exon is relevant for its activity. These results are in line with a CLIP-seq study that drew an RNA map of hnRNPM-mediated splicing repression, which required its binding proximal to or within exons (50). Our work now indicates that, differently from what reported for other splicing regulators (44), the presence of a distal binding site for hnRNPM is not sufficient to influence splicing outcome (Figure 6D), strengthening the hypothesis of position-based activity for hnRNPM-mediated splicing regulation.

The splicing reaction proceeds through three stages before splice site pairing is committed (32). In the first stage, referred to as H complex, RBPs assemble on the pre-mRNA. In the next stage, referred to as E complex, the U1 snRNP and SR proteins assemble on the splice sites and within the exons. In the third stage, referred to as A complex, the branch point is recognized by the U2 snRNP, which leads to splice site pairing and commitment to a specific splicing choice (32). Our results showing increased interaction with U170K upon inhibition of the PI3K/AKT/mTOR pathway suggest that hnRNPM might affect early stages of spliceosome assembly by influencing the U1 snRNP recruitment to the 5′ splice site.

HnRNPM was recently proposed to induce epithelial to mesenchymal transition (EMT) and maintenance of a mesenchymal phenotype in breast cancer (48). HnRNPM expression was significantly associated with gene signatures of aggressive breast cancer, it was elevated in breast cancer patient's specimens, and it was positively correlated with breast tumor mesenchymal status, thus indicating its contribution to breast cancer metastasis (48). Sarcomas are thought to arise from mesenchymal cells and do not have a baseline epithelial phenotype as seen in many carcinomas. This fact excludes sarcomas from the EMT-MET metastasis paradigm whereby tumor cells in carcinomas must lose their epithelial features to escape the primary tumor, but regain them to colonize the secondary site (66). ES cells maintain an intermediate phenotype with features of both epithelial and mesenchymal cells, but without activation of their complete gene program associated with either phenotype. In particular, the high level of ZEB2 in sarcomas prevents epithelial differentiation, whereas EWS-FLI-1 inhibits full mesenchymal differentiation (66). Accordingly, ES mesenchymal features become more pronounced with EWS-FLI-1 knockdown (67). Hence, although BEZ235 treatment induced hnRNPM upregulation in ES cells, this regulation was not associated with EMT (data not shown) as in breast cancer (48).

Upregulation of hnRNPM upon BEZ235 treatment correlated with splicing changes in genes involved in cellular junctions, spliceosome and p53/FoxO and MAPK signaling pathways that are enriched in hnRNPM binding sites near the regulated exons (Supplementary Figure S6A). Since hnRNPM knockdown abolishes most of these events (Figure 6), it is likely that it directly participates to their splicing regulation upon inhibition of the PI3K/AKT/mTOR pathway. Indeed, CLIP experiments indicated that hnRNPM binds in proximity of regulated exons and that this interaction is promoted by BEZ235. Interestingly, more than 80% of the splicing-regulated genes containing hnRNPM consensus motifs are also candidate targets of hnRNPK (Supplementary Table S8), which is one of the main potential regulators of the splicing response to BEZ235 from our bioinformatics analysis. Remarkably, hnRNPK co-sediments with U1 and U2AF splicing factors but its subnuclear localization was not affected by PI3K/AKT/mTOR inhibition. These results highlight an hnRNPs-orchestrated splicing response induced by inhibition of the PI3K/AKT/mTOR signaling pathway, counteracting SR proteins activity (68–70). Although other splicing factors were identified by our analyses and are likely involved in the global changes in AS elicited by inhibition of the PI3K/AKT/mTOR pathway, our findings point to a key role for hnRNPM in this process.

We found a correlation between hnRNPM expression and the resistance of ES cell lines to BEZ235 treatment;

in fact, hnRNPM was significantly more expressed in the more resistant LAP35 and TC71 cell lines than in the SKNMC cells. Furthermore, high hnRNPM expression was associated to decrease in the overall survival (*P*-value = 1.17E–03) of sarcoma patients. Accordingly, downregulation of hnRNPM expression was sufficient to sensitize ES cells to BEZ235 treatment. It was recently reported that hnRNPM directly interacts with Rictor, thus cooperating with the mTORC2 complex in downstream functions through the phosphorylation of SGK1. Notably, overexpression of hnRNPM rescued the phosphorylation of SGK1 upon Rictor depletion (71). Thus, hnRNPM upregulation may allow cancer cells to escape PI3K/AKT/mTOR pathway by maintaining active the SGK1/FoxO signaling pathway. On the other hand, the activity of core spliceosomal components and accessory splicing factors is highly modulated by post-translational modifications, such as reversible phosphorylation (46). Thus, it is also possible that PI3K/AKT/mTOR inhibition partly elicits transcriptome reprogramming by modulating the activity of kinases and phosphatases involved in splicing regulation.

Collectively, our work establishes the hnRNPM–regulated splicing program as a novel molecular pathway that drives resistance to the inhibition of PI3K/AKT/mTOR signaling pathway, suggesting that it might be targeted to improve clinical response to currently used chemotherapeutic regimens in ES patients.

DATA AVAILABILITY

The HTA2 data have been deposited in the GEO database under ID GEO: GSE93579.

SUPPLEMENTARY DATA

Supplementary Data are available at NAR Online.

ACKNOWLEDGEMENTS

The authors wish to thank Drs Pierre de la Grange and Olivier Ariste (Genosplice, Paris) for microarray analyses, Dr Elisabetta Volpe for assistance in PI analysis, and Prof. Claudio Sette for critical reading of the manuscript.

FUNDING

Associazione Italiana Ricerca sul Cancro (AIRC) [IG17278 to M.P.P.]; Association for International Cancer Research [AICR-UK 14-0333 to M.P.P]; Ministry of Health 'Ricerca Corrente' and '5 × 1000 Anno 2014' (to Fondazione Santa Lucia). Funding for open access charge: AIRC [IG17278].
Conflict of interest statement. None declared.

REFERENCES

1. Lessnick,S.L., Braun,B.S., Denny,C.T. and May,W.A. (1995) Multiple domains mediate transformation by the Ewing's sarcoma EWS/FLI-1 fusion gene. *Oncogene*, **10**, 423–431.
2. Delattre,O., Zucman,J., Plougastel,B., Desmaze,C., Melot,T., Peter,M., Kovar,H., Joubert,I., de Jong,P., Rouleau,G. *et al.* (1992) Gene fusion with an ETS DNA-binding domain caused by chromosome translocation in human tumours. *Nature*, **359**, 162–165.
3. Dutertre,M., Sanchez,G., De Cian,M.C., Barbier,J., Dardenne,E., Gratadou,L., Dujardin,G., Le Jossic-Corcos,C., Corcos,L. and Auboeuf,D. (2010) Cotranscriptional exon skipping in the genotoxic stress response. *Nat. Struct. Mol. Biol.*, **17**, 1358–1366.
4. Paronetto,M.P., Miñana,B. and Valcárcel,J. (2011) The Ewing sarcoma protein regulates DNA damage-induced alternative splicing. *Mol. Cell*, **43**, 353–368.
5. Paronetto,M.P., Bernardis,I., Volpe,E., Bechara,E, Sebestyén,E., Eyras,E. and Valcárcel,J. (2014) Regulation of FAS exon definition and apoptosis by the Ewing sarcoma protein. *Cell Rep.*, **7**, 1211–1226.
6. Paronetto,M.P. (2013) Ewing sarcoma protein: a key player in human cancer. *Int. J. Cell Biol.*, 642853.
7. Li,Y., Luo,H., Liu,T., Zacksenhaus,E. and Ben-David,Y. (2015) The ets transcription factor Fli-1 in development, cancer and disease. *Oncogene*, **34**, 2022–2031.
8. Riggi,N. and Stamenkovic,I. (2007) The Biology of Ewing sarcoma. *Cancer Lett.*, **254**, 1–10.
9. Shankar,A.G., Pinkerton,C.R., Atra,A., Ashley,S., Lewis,I., Spooner,D., Cannon,S., Grimer,R., Cotterill,S.J. and Craft,A.W. (1999) Local therapy and other factors influencing site of relapse in patients with localised Ewing's sarcoma. United Kingdom Children's Cancer Study Group (UKCCSG). *Eur. J. Cancer*, **35**, 1698–1704.
10. Bacci,G., Mercuri,M., Longhi,A., Bertoni,F., Barbieri,E., Donati,D., Giacomini,S., Bacchini,P., Pignotti,E., Forni,C. *et al.* (2002) Neoadjuvant chemotherapy for Ewing's tumour of bone: recent experience at the Rizzoli Orthopaedic Institute. *Eur. J. Cancer*, **38**, 2243–2251.
11. Linabery,A.M. and Ross,J.A. (2008) Childhood and adolescent cancer survival in the US by race and ethnicity for the diagnostic period 1975–1999. *Cancer*, **113**, 2575–2596.
12. Pishas,K.I. and Lessnick,S.L. (2016) Recent advances in targeted therapy for Ewing sarcoma. *F1000Res.*, **5**, doi:10.12688/f1000research.8631.1.eCollection 2016.
13. Toomey,E.C., Schiffman,J.D. and Lessnick,S.L. (2010) Recent advances in the molecular pathogenesis of Ewing's sarcoma. *Oncogene*, **29**, 4504–4516.
14. Mateo-Lozano,S., Tirado,O.M. and Notario,V. (2003) Rapamycin induces the fusion-type independent downregulation of the EWS/FLI-1 proteins and inhibits Ewing's sarcoma cell proliferation. *Oncogene*, **22**, 9282–9287.
15. Manara,M.C., Nicoletti,G., Zambelli,D., Ventura,S., Guerzoni,C., Landuzzi,L., Lollini,P.L., Maira,S.M., García-Echeverría,C., Mercuri,M. *et al.* (2010) NVP-BEZ235 as a new therapeutic option for sarcomas. *Clin. Cancer Res.*, **16**, 530–540.
16. Mamane,Y., Petroulakis,E., LeBacquer,O. and Sonenberg,N. (2006) mTOR, translation initiation and cancer. *Oncogene*, **25**, 6416–6422.
17. Cornu,M., Albert,V. and Hall,M.N. (2013) mTOR in aging, metabolism, and cancer. *Curr. Opin. Genet. Dev.*, **23**, 53–62.
18. Fruman,D.A. and Rommel,C. (2014) PI3K and cancer: lessons, challenges and opportunities. *Nat. Rev. Drug Discov.*, **13**, 140–156.
19. Saxton,R.A. and Sabatini,D.M. (2017) mTOR signaling in growth, metabolism, and disease. *Cell*, **168**, 960–976.
20. Hay,N. and Sonenberg,N. (2004) Upstream and downstream of mTOR. *Genes Dev.*, **18**, 1926–1945.
21. Petricoin,E.F. III, Espina,V., Araujo,R.P., Midura,B., Yeung,C., Wan,X., Eichler,G.S., Johann,D.J. Jr, Qualman,S., Tsokos,M. *et al.* (2007) Phosphoprotein pathway mapping: Akt/mammalian target of rapamycin activation is negatively associated with childhood rhabdomyosarcoma survival. *Cancer Res.*, **67**, 3431–3440.
22. Scotlandi,K. and Picci,P. (2008) Targeting insulin-like growth factor 1 receptor in sarcomas. *Curr. Opin. Oncol.*, **20**, 419–427.
23. Yu,H., Ge,Y., Guo,L. and Huang,L. (2017) Potential approaches to the treatment of Ewing's sarcoma. *Oncotarget*, **8**, 5523–5539.
24. Mita,M.M., Mita,A.C., Chu,Q.S, Rowinsky,E.K., Fetterly,G.J., Goldston,M., Patnaik,A., Mathews,L., Ricart,A.D., Mays,T. *et al.* (2008) Phase I trial of the novel mammalian target of rapamycin inhibitor deforolimus (AP23573; MK-8669) administered intravenously daily for 5 days every 2 weeks to patients with advanced malignancies. *J. Clin. Oncol.*, **26**, 361–367.
25. Huang,Z., Wu,Y., Zhou,X., Qian,J., Zhu,W., Shu,Y. and Liu,P. (2015) Clinical efficacy of mTOR inhibitors in solid tumors: a systematic review. *Future Oncol.*, **11**, 1687–1699.
26. Sun,S.Y., Rosenberg,L.M., Wang,X., Zhou,Z., Yue,P., Fu,H. and Khuri,F.R. (2005) Activation of Akt and eIF4E survival pathways by

rapamycin-mediated mammalian target of rapamycin inhibition. *Cancer Res.*, **65**, 7052–7058.
27. O'Reilly,K.E., Rojo,F., She,Q.B., Solit,D., Mills,G.B., Smith,D., Lane,H., Hofmann,F., Hicklin,D.J., Ludwig,D.L. *et al.* (2006) mTOR inhibition induces upstream receptor tyrosine kinase signaling and activates Akt. *Cancer Res.*, **66**, 1500–1508.
28. Passacantilli,I., Capurso,G., Archibugi,L., Calabretta,S., Caldarola,S., Loreni,F., Delle Fave,G. and Sette,C. (2014) Combined therapy with RAD001 e BEZ235 overcomes resistance of PET immortalized cell lines to mTOR inhibition. *Oncotarget*, **5**, 5381–5391.
29. Ni,J., Ramkissoon,S.H., Xie,S., Goel,S., Stover,D.G., Guo,H., Luu,V., Marco,E., Ramkissoon,L.A., Kang,Y.J. *et al.* (2016) Combination inhibition of PI3K and mTORC1 yields durable remissions in mice bearing orthotopic patient-derived xenografts of HER2-positive breast cancer brain metastases. *Nat. Med.*, **22**, 723–726.
30. Sandhöfer,N., Metzeler,K.H., Rothenberg,M., Herold,T., Tiedt,S., Groiß,V., Carlet,M., Walter,G., Hinrichsen,T., Wachter,O. *et al.* (2015) Dual PI3K/mTOR inhibition shows antileukemic activity in MLL-rearranged acute myeloid leukemia. *Leukemia*, **29**, 828–838.
31. Paronetto,M.P., Passacantilli,I. and Sette,C. (2016) Alternative splicing and cell survival: from tissue homeostasis to disease. *Cell Death Differ.*, **23**, 1919–1929.
32. Wahl,M.C., Will,C.L. and Lührmann,R. (2009) The spliceosome: design principles of a dynamic RNP machine. *Cell*, **136**, 701–718.
33. Black,D.L. (2003) Mechanisms of alternative pre-messenger RNA splicing. *Annu. Rev. Biochem.*, **72**, 291–336.
34. Matlin,A.J., Clark,F. and Smith,C.W. (2005) Understanding alternative splicing: towards a cellular code. *Nat. Rev. Mol. Cell Biol.*, **6**, 386–398.
35. Chen,M. and Manley,J.L. (2009) Mechanisms of alternative splicing regulation: insights from molecular and genomics approaches. *Nat. Rev. Mol. Cell Biol.*, **10**, 741–754.
36. Pan,Q., Saltzman,A.L., Kim,Y.K., Misquitta,C., Shai,O., Maquat,L.E., Frey,B.J. and Blencowe,B.J. (2006) Quantitative microarray profiling provides evidence against widespread coupling of alternative splicing with nonsense-mediated mRNA decay to control gene expression. *Genes Dev.*, **20**, 153–158.
37. Zhang,C., Li,H.R., Fan,J.B., Wang-Rodriguez,J., Downs,T., Fu and Zhang,M.Q. (2006) Profiling alternatively spliced mRNA isoforms for prostate cancer classification. *BMC Bioinformatics*, **7**, 202.
38. Klinck,R., Bramard,A., Inkel,L., Dufresne-Martin,G., Gervais-Bird,J., Madden,R., Paquet,E.R., Koh,C., Venables,J.P., Prinos,P. *et al.* (2008) Multiple alternative splicing markers for ovarian cancer. *Cancer Res.*, **68**, 657–663.
39. Venables,J.P., Klinck,R., Bramard,A., Inkel,L., Dufresne-Martin,G., Koh,C., Gervais-Bird,J., Lapointe,E., Froehlich,U., Durand,M. *et al.* (2008) Identification of alternative splicing markers for breast cancer. *Cancer Res.*, **68**, 9525–9531.
40. Bland,C.S., Wang,E.T., Vu,A., David,M.P., Castle,J.C., Johnson,J.M., Burge,C.B. and Cooper,T.A. (2010) Global regulation of alternative splicing during myogenic differentiation. *Nucleic Acids Res.*, **38**, 7651–7664.
41. Maira,S.M., Stauffer,F., Brueggen,J., Furet,P., Schnell,C., Fritsch,C., Brachmann,S., Chène,P., De Pover,A., Schoemaker,K. *et al.* (2008) Identification and characterization of NVP-BEZ235, a new orally available dual phosphatidylinositol 3-kinase/mammalian target of rapamycin inhibitor with potent in vivo antitumor activity. *Mol. Cancer Ther.*, **7**, 1851–1863.
42. Smith,C.W. and Valcárcel,J. (2000) Alternative pre-mRNA splicing: the logic of combinatorial control. *Trends Biochem. Sci.*, **25**, 381–388.
43. Matera,A.G. and Wang,Z. (2014) A day in the life of the spliceosome. *Nat. Rev. Mol. Cell Biol.*, **15**, 108–121.
44. Fu,X.D. and Ares,M. Jr (2014) Context-dependent control of alternative splicing by RNA-binding proteins. *Nat. Rev. Genet.*, **15**, 689–701.
45. Witten,J.T. and Ule,J. (2011) Understanding splicing regulation through RNA splicing maps. *Trends Genet.*, **27**, 89–97.
46. Naro,C. and Sette,C. (2013) Phosphorylation-mediated regulation of alternative splicing in cancer. *Int. J. Cell. Biol.*, 151839.
47. Fidaleo,M., Svetoni,F., Volpe,E., Miñana,B., Caporossi,D. and Paronetto,M.P. (2015) Genotoxic stress inhibits Ewing sarcoma cell growth by modulating alternative pre-mRNA processing of the RNA helicase DHX9. *Oncotarget*, **6**, 31740–31757.
48. Xu,Y., Gao,X.D., Lee,J.H., Huang,H., Tan,H., Ahn,J., Reink,L.M., Peter,M.E., Feng,Y., Gius,D. *et al.* (2014) Cell type-restricted activity of hnRNPM promotes breast cancer metastasis via regulating alternative splicing. *Genes Dev.*, **28**. 1191–1203.
49. Damianov,A., Ying,Y., Lin,C.H., Lee,J.A., Tran,D., Vashisht,A.A., Bahrami-Samani,E., Xing,Y., Martin,K.C., Wohlschlegel,J.A. *et al.* (2016). Rbfox proteins regulate splicing as part of a large multiprotein complex LASR. *Cell*, **165**, 606–619.
50. Huelga,S.C., Vu,A.Q., Arnold,J.D., Liang,T.Y., Liu,P.P., Yan,B.Y., Donohue,J.P., Shiue,L., Hoon,S., Brenner,S. *et al.* (2012) Integrative genome-wide analysis reveals cooperative regulation of alternative splicing by hnRNP proteins. *Cell Rep.*, **1**, 167–178.
51. Stricker,T.P., Brown,C.D., Bandlamudi,C., McNerney,M., Kittler,R., Montoya,V., Peterson,A., Grossman,R. and White,K.P. (2017) Robust stratification of breast cancer subtypes using differential patterns of transcript isoform expression. *PLoS Genet.*, **13**, e1006589.
52. Bonnal,S., Vigevani,L. and Valcárcel,J. (2012) The spliceosome as a target of novel antitumour drugs. *Nat. Rev. Drug Discov.*, **11**, 847–859.
53. Lee,S.C. and Abdel-Wahab,O. (2016) Therapeutic targeting of splicing in cancer. *Nat. Med.*, **22**, 976–986.
54. Hartford,C.M. and Ratain,M.J. (2007) Rapamycin: something old, something new, sometimes borrowed and now renewed. *Clin. Pharmacol. Ther.*, **82**, 381–388.
55. Cai,Y., Dodhia,S. and Su,G.H. (2017) Dysregulations in the PI3K pathway and targeted therapies for head and neck squamous cell carcinoma. *Oncotarget*, **8**, 22203–22217.
56. Mayer,I.A. and Arteaga,C.L. (2016) The PI3K/AKT pathway as a target for cancer treatment. *Annu. Rev. Med.*, **67**, 11–28.
57. Kim,L.C., Cook,R.S. and Chen,J. (2017) mTORC1 and mTORC2 in cancer and the tumor microenvironment. *Oncogene.*, **36**, 2191–2201.
58. Slotkin,E.K., Patwardhan,P.P., Vasudeva,S.D., de Stanchina,E., Tap,W.D. and Schwartz,G.K. (2015) MLN0128, an ATP-competitive mTOR kinase inhibitor with potent in vitro and in vivo antitumor activity, as potential therapy for bone and soft-tissue sarcoma. *Mol. Cancer Ther.*, **14**, 395–406.
59. Gobin,B., Battaglia,S., Lanel,R., Chesneau,J., Amiaud,J., Rédini,F., Ory,B. and Heymann,D. (2014) NVP-BEZ235, a dual PI3K/mTOR inhibitor, inhibits osteosarcoma cell proliferation and tumor development in vivo with an improved survival rate. *Cancer Lett.*, **344**, 291–298.
60. Martinez-Contreras,R., Cloutier,P., Shkreta,L., Fisette,J.F., Revil,T. and Chabot,B. (2007) hnRNP proteins and splicing control. *Adv. Exp. Med. Biol.*, **623**, 123–147.
61. Swanson,M.S. and Dreyfuss,G. (1988) RNA binding specificity of hnRNP proteins: a subset bind to the 3′ end of introns. *EMBO J.*, **7**, 3519–3529.
62. Datar,K.V., Dreyfuss,G. and Swanson,M.S. (1993) The human hnRNP M proteins: identification of a methionine/arginine-rich repeat motif in ribonucleoproteins. *Nucleic Acids Res.*, **21**, 439–446.
63. Hovhannisyan,R.H. and Carstens,R.P. (2007) Heterogeneous ribonucleoprotein m is a splicing regulatory protein that can enhance or silence splicing of alternatively spliced exons. *J. Biol. Chem.*, **282**, 36265–33674.
64. Kafasla,P., Patrinou-Georgoula,M., Lewis,J.D. and Guialis,A. (2002) Association of the 72/74-kDa proteins, members of the heterogeneous nuclear ribonucleoprotein M group, with the pre-mRNA at early stages of spliceosome assembly. *Biochem. J.*, **363**, 793–799.
65. Rappsilber,J., Ryder,U., Lamond,A.I. and Mann,M. (2002) Large-scale proteomic analysis of the human spliceosome. *Genome Res.*, **12**, 1231–1245.
66. Wiles,E.T., Bell,R., Thomas,D., Beckerle,M. and Lessnick,S.L. (2013) ZEB2 represses the epithelial phenotype and facilitates metastasis in Ewing sarcoma. *Genes Cancer*, **4**, 486–500.
67. Chaturvedi,A., Hoffman,L.M., Welm,A.L., Lessnick,S.L. and Beckerle,M.C. (2012) The EWS/FLI oncogene drives changes in cellular morphology, adhesion, and migration in Ewing sarcoma. *Genes Cancer*, **3**, 102–116.
68. Blaustein,M., Pelisch,F., Tanos,T., Muñoz,M.J., Wengier,D., Quadrana,L., Sanford,J.R., Muschietti,J.P., Kornblihtt,A.R., Cáceres,J.F. *et al.* (2005) Concerted regulation of nuclear and cytoplasmic activities of SR proteins by AKT. *Nat. Struct. Mol. Biol.*, **12**, 1037–1044.

69. Zhou,Z., Qiu,J., Liu,W., Zhou,Y., Plocinik,R.M., Li,H., Hu,Q., Ghosh,G., Adams,J.A., Rosenfeld,M.G. *et al.* (2012) The Akt-SRPK-SR axis constitutes a major pathway in transducing EGF signaling to regulate alternative splicing in the nucleus. *Mol. Cell*, **47**, 422–433.
70. Wang,P., Zhou,Z., Hu,A., Ponte de Albuquerque,C., Zhou,Y., Hong,L., Sierecki,E., Ajiro,M., Kruhlak,M., Harris,C. *et al.* (2014) Both decreased and increased SRPK1 levels promote cancer by interfering with PHLPP-mediated dephosphorylation of Akt. *Mol. Cell*, **54**, 378–391.
71. Chen,W.Y., Lin,C.L., Chuang,J.H., Chiu,F.Y., Sun,Y.Y., Liang,M.C. and Lin,Y. (2017) Heterogeneous nuclear ribonucleoprotein M associates with mTORC2 and regulates muscle differentiation. *Sci. Rep.*, **7**, 41159.
72. Pandya-Jones,A. and Black,D.L. (2009) Co-transcriptional splicing of constitutive and alternative exons. *RNA*, **15**, 1896–1908.